53rd AIAA/ASME/ASCE/AHS/ASC Structures, Structural Dynamics and Materials Conference
20th AI
23 - 26 April 2012, Honolulu, Hawaii

AIAA 2012-1636

CFD-CSD Coupled Aeroelastic Analysis of Flexible Flapping Wings for MAV Applications: Methodology Validation

Ria Malhan*
Vinod K. Lakshminarayan†
James Baeder‡ Inderjit Chopra§
Pierangelo Masarati¶ Marco Morandini‖ Giuseppe Quaranta**

A coupled CFD-CSD solver is used to simulate the aerodynamics of a flexible flapping wing. The CFD solver is a compressible RANS solver. The free general-purpose multi-body dynamics solver MBDyn is used as the structural solver after an extension to take into account non linear shell straining, making it possible to analyze plates with large deformations. Validation of the two codes for flapping wings/plates is carried out independently. The solvers are then coupled and validated against prior experiments and analysis on a spanwise flexible wing at $Re = 30,000$. It is observed that due to flexibility, the average chordwise propulsive force, C_T increases by 47% as a result of increase in plunge amplitude, effective angle of attack and leading edge suction towards the outer sections as compared to for a rigid wing. Additionally, the flexible wing has higher 3D flow. Then, a chordwise flexible root flapping wing is analyzed using the solver at $Re = 10,000$. As a result of the flexibility, camber is induced in the wing as it flaps. Highly 3D flow was observed with the strength of the vortices increasing from root to tip. Due to camber in the wing, the resultant force is vectored more in the chordwise direction as compared to for rigid wings, which results in higher thrust. The average C_T increased by 25% and average C_L increased by 10%. The current work demonstrates the capability of an aeroelastic solver to characterize the flowfield of a flexible flapping wing MAV in 3D.

Nomenclature

a	Speed of sound, m/s
AR	Aspect Ratio
b	Span length, m
c	Airfoil chord, m
C_d	Drag force coefficient
C_l	Lift force coefficient
f	Flapping frequency, Hz
h	Plunge displacement (non dim. by chord)
h_o	Plunge amplitude (non dim. by chord)
k	Reduced frequency
M_∞	Free stream Mach number, U_∞/a
Re	Reynolds number
U_∞	Free stream velocity, m/s

*Graduate Research Assistant, Department of Aerospace Engineering, University of Maryland, rmalhan@umd.edu
†Postdoctoral Fellow, Department of Aeronautics and Astronautics, Stanford University, vinodkl@stanford.edu
‡Associate Professor, Department of Aerospace Engineering, University of Maryland, baeder@umd.edu
§Alfred Gessow Professor, Department of Aerospace Engineering, University of Maryland, chopra@umd.edu
¶Associate Professor, Dipartimento di Ingegneria Aerospaziale, Politecnico di Milano, masarati@aero.polimi.it
‖Assistant Professor, Dipartimento di Ingegneria Aerospaziale, Politecnico di Milano, morandini@aero.polimi.it
**Assistant Professor, Dipartimento di Ingegneria Aerospaziale, Politecnico di Milano, giuseppe.quaranta@polimi.it

U_{tip} Tip speed, m/s
α Angle of attack
γ_o Flapping amplitude, deg
γ Flapping angle, deg
ϕ Phase difference between pitch and plunge, deg
θ Pitch angle, deg
θ_o Fixed pitch angle, deg
θ_a Pitch amplitude, deg

I. Introduction

Micro air vehicles (MAV) offer a great potential for exploration, communication, surveillance and reconnaissance missions especially in constrained environments. In order to carry out these various missions, MAVs should be efficient, maneuverable and capable of hover. Due to their small size, they operate at low Reynolds numbers. They can be classified into three broad categories: fixed wing, rotary wing and bio-inspired flapping wing vehicles. The fixed wing and rotary wing MAVs are scaled down versions of the traditional full scale concepts. Fixed wing MAVs are efficient; however, they lack the ability to hover and thus they are unsuitable for operations in confined spaces. Rotary wing MAVs are hover capable; however, they have lower efficiency as compared to fixed wing MAVs.[1] This implies that it may not be beneficial to just scale down full scale concepts. Since MAVs operate in the Reynolds number regime of $10,000$-$100,000$, which is about the same at which large insects and small birds operate, it may be beneficial to take inspiration from natural flyers to learn their flight physics.

There have been a number of experimental studies to understand the aerodynamics of flapping wings. Knoller and Betz[2,3] were the first to identify that positive propulsive thrust is produced due to pure plunging motion of a wing in free-stream as it results in an effective angle of attack during both the up-stroke and down-stroke. The directions of lift and thrust are shown in Figure 1. Katzmayer experimentally verified this fact in 1922 by measuring the thrust from a stationary wing placed in a sinusoidally oscillating wind stream.[4] Pitching/plunging airfoils at high Reynolds numbers (on the order of million) were studied in detail while investigating dynamic stall of helicopter blades. The formation of a leading edge vortex due to flow separation was found to have significant effect on the blade aerodynamics. This leads to forces and moments that are very different from static stall values. McCroskey[5] and Carr[6] provided comprehensive reviews on this topic. While this work can serve as a starting point for investigating flapping wing MAV aerodynamics, the Reynolds number regime is at least one to two orders of magnitude higher.

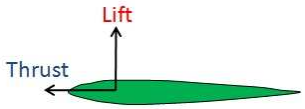

Figure 1. Definition of lift and thrust

Recently, several experiments have been performed in the lower Reynolds number regime on flapping wings. Since MAV flapping wings generally have a very low aspect ratio, it may be expected that 3D effects will have an important role to play. Hart et al.[7] experimentally measured the instantaneous lift and drag of a pitching and plunging small aspect ratio rigid wing and also included PIV measurement of the flow-field at one spanwise location. Even though this study provides good data for computational validation, it does not provide much insight into the flow physics. Recently, experiments have also been carried out by Yuan et al.[8] on root based flapping, which closely mimic the kinematics of avian flight. These experiments measured instantaneous forces over a flap cycle. However, it should be noted that all these studies were based on rigid wings. In nature, the wings of birds and insects are extremely light weight and highly flexible which may be beneficial aerodynamically. It has been reported in the literature that wing chordwise flexibility can result in significant improvements in thrust produced by flapping wings. For instance the experimental study done by Wang et al.[9] showed that dragonflies can produce a camber of upto 0.2 chord to improve their aerodynamic efficiency. Malhan et al.[10] and Wu et al.[11] recently carried out experiments on flexible flapping wings. Even though experiments can provide a wealth of information, it is extremely challenging to carry out detailed

flow measurement and hence to understand the flow physics at low Reynolds numbers.

CFD is an alternative tool that can be used in conjunction with experiments to understand the flow physics. Various studies have been carried out on 2D pitching/plunging airfoils.[12–14] However, limited work has been done on 3D flapping wings. For example, Yuan et al.,[8] simulate their root flapping experiments on rigid wings (mentioned earlier). Recently, there have been some studies which include the effects of wing flexibility while trying to understand the aerodynamics of flapping wings.[15,16] Experiments carried out by Heathcote et al.[17] serve as a benchmark case where the effect of spanwise flexibility on aerodynamics was investigated. Chordwise flexibility was investigated by Gopalakrishnan et al.,[18] however, their analysis was limited to linear straining of the membrane. The focus of the current work is to extend the limited body of work on 3D flapping wing simulations and develop computational methodologies to study the performance and flow physics of realistic flexible flapping wing MAVs. Earlier work by Lakshminarayan and Baeder[19–21] demonstrated the capability of using a compressible Reynolds Averaged Navier-Stokes (RANS) solver to study the flow physics of hovering micro-rotors. This solver was further extended to simulate rigid flapping wings.[22] CFD methodology validation was carried out first for pitching/plunging airfoils in 2D flow environment at different Reynolds numbers. Next, a rigid wing with root based flapping motion was simulated in 3D and validated against the results published by Yuan et al.[8] The aim of this work will be to expand the current capabilities to include the wing flexibility as well, and study its effects on aerodynamic performance and efficiency. Unlike the previous literature,[18] this work is not limited to analyze a shell/membrane with linear straining and can handle large deformations essential to analyze realistic flapping wing MAVs.

II. Numerical Approach

To obtain reliable predictions of a flexible flapping wing performance and the detailed aerodynamic environment surrounding the wing, both the fluid and the structural domains need to be modeled accurately. Solving the two domains in a single monolithic solver is impractical, instead a coupled simulation using specialized solvers allows modeling of domain-specific features in a simpler, efficient manner. Interactions between the fluid and the structural surface can then be modeled by exchanging information at the fluid-structure interface. The present work uses such a coupled simulation where independent CFD and CSD solvers are used together. The CFD solver, structural solver, and coupling methodology are described here.

II.A. Aerodynamic Model

3D simulations of the flapping wing are done using OVERTURNS,[21] a compressible structured overset RANS solver developed in-house at the University of Maryland. This code solves the compressible RANS equations using the diagonal form of the implicit approximate factorization method developed by Pulliam and Chaussee[23] with second order accuracy in time. The inviscid terms are computed using a third-order MUSCL scheme with Roe flux difference splitting and Korens limiter, and the viscous terms are computed using second-order central differencing. Time accurate low Mach preconditioning in dual-time scheme described by Buelow et al.[24] and Pandya et al.[25] is used. Preconditioning is used not only to improve convergence, but also to improve accuracy. Spalart-Allmaras[26] turbulence model is employed for RANS closure. This code has the capability to use overset meshes to capture the flow features better. Implicit hole-cutting method developed by Lee[27] and refined by Lakshminarayan[21] is used to find the connectivity information between the overset meshes.

II.B. Structural Model

The structural analysis is based on MBDyn which is a free general purpose multibody software developed at Politecnico di Milano and recently enhanced by adding support for nonlinear 2D structural elements (shells,[28] with membranes under development) and generic Fluid-Structure Interaction (FSI) capabilities.[28,29] This solver is enhanced by the capability to directly account for the nonlinear structural dynamics of shells, in addition to the existing support for nonlinear beams. This allows us to consider highly flexible flapping wings with large deformations. MBDyn was already coupled in a general form to a Vortex Lattice (VL) free wake analysis called NUVOLA for rotorcraft applications[30] and to an incompressible unsteady DNS and URANS solvers.[29] The original approach has been generalized and abstracted, to ease its adaptation to different external solvers; for this purpose, a python interface has been added. The use of a general purpose multibody approach provides the user freedom in defining the mechanical part of the problem. This is especially true in

MAV analysis when one needs to consider the mechanism that is used to actuate the aerodynamic surfaces, possibly including its compliance. The analysis is based on the direct integration in time of an Initial Value Problem (IVP) that describes the dynamics of a set of arbitrarily interconnected bodies. Compliant connectivity is realized in the form of nonlinear finite elements, using beam[31] and shell[28] elements, while kinematic constraints are modeled by algebraic relationships enforced using Lagrange multipliers.

II.C. Coupling Strategy

A Python-based computational framework that facilitates the data exchange between the participating solvers is used. This coupling algorithm allows exchange of motion (which is the kinematics mapping from the CSD to the CFD solver) and loads (from the CFD to the CSD solver) at the fluid-structure interface. This exchange in principle is done in a tight manner, that is at each iteration of the nonlinear problem solution procedure for a given time step, although to reduce the computational cost it is relaxed as soon as it is allowed by the relative compliance of the coupled problems. Coupling between the two codes was done using a first order and also a staggered second order accurate approach which satisfies the discrete geometric conservation law (DGCL) presented by Farhat et al.[32] However, it was observed that both the approaches gave similar results. The domains and meshes of the two solvers are non conformal. The mapping of these incompatible domains is based on an original scheme that preserves the work exchanged between the structural and the aerodynamic domains.[33] This mapping is based on a Moving Least Squares (MLS) fitting of the discretization of the interface between the two domains using a compact support that consists of Radial Basis Functions (RBF).

III. 3D CFD Code Validation for Pitching and Plunging Wings

OVERTURNS was first validated for rigid flapping wings in a 3D flow environment using a rigid flapping wing fixed at the root in an earlier paper presented by the current authors.[22] A brief summary of the study is presented here. A spanwise tapered wing with NACA 0005 airfoil cross section which was experimentally studied by Yuan et al.[8] at the National Research Council (NRC) in a water tunnel, was simulated. The water tunnel had a 15 in (width) × 20 in (height) test section. The wing has a span of 0.35 m, root chord of 0.09 m and tip chord of 0.07 m. The reference section is chosen at a spanwise position of 0.25 m (71% of the span) and has a chord of 0.07 m. The flap kinematics are as follows:

Flap: $\gamma = \gamma_o \cos(2 \cdot \pi f \cdot t)$,

Pitch: $\theta = \text{-}\theta_a \sin(2 \cdot \pi f \cdot t)$, with flap amplitude, $\gamma_o = 15°$ and pitch amplitude, $\theta_a = 40°$. Note that γ and θ are positive flap up and nose up, respectively. The flapping frequency is 0.46 Hz. The reduced frequency at the reference section is 1.6, based on reference chord and maximum tip velocity. The wing is pitched about the leading edge. The freestream velocity is 0.0635 m/s and the maximum tip velocity is 0.264 m/s. The reference velocity with which all the quantities are normalized is given by $\sqrt{(0.0635^2 + 0.264^2)} = 0.2715$ m/s. The Reynolds number at the reference section is about 19,000 (based on the reference section chord

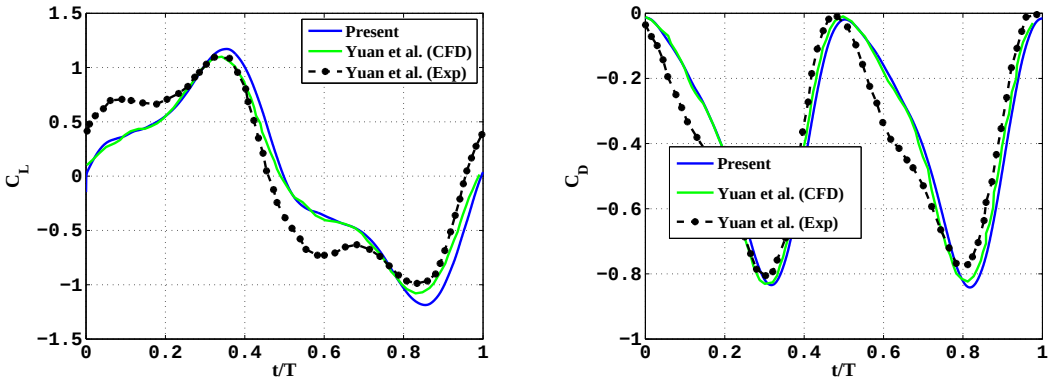

(a) C_L (b) C_D

Figure 2. Instantaneous C_L and C_D variation over a flap cycle for root flapping case (rigid wing)

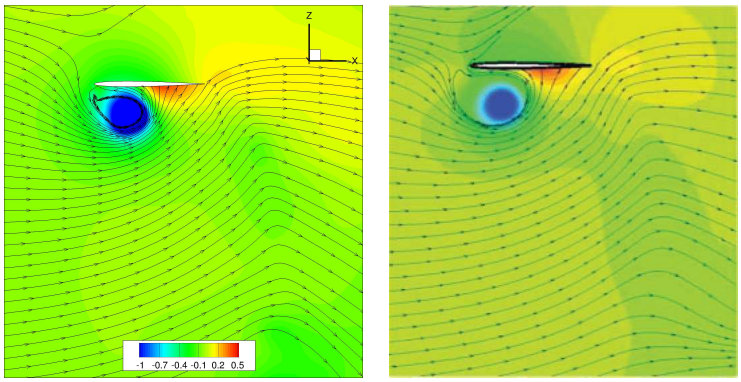

(a) t=0, Present (b) t=0, Yuan et al.

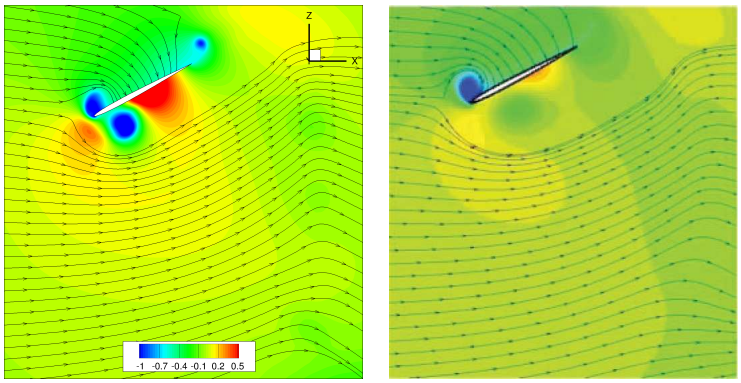

(c) t=T/8, Present (d) t=T/8, Yuan et al.

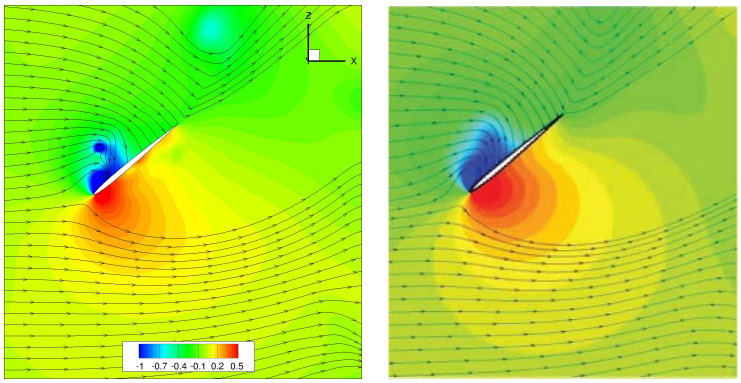

(e) t=T/4, Present (f) t=T/4, Yuan et al.

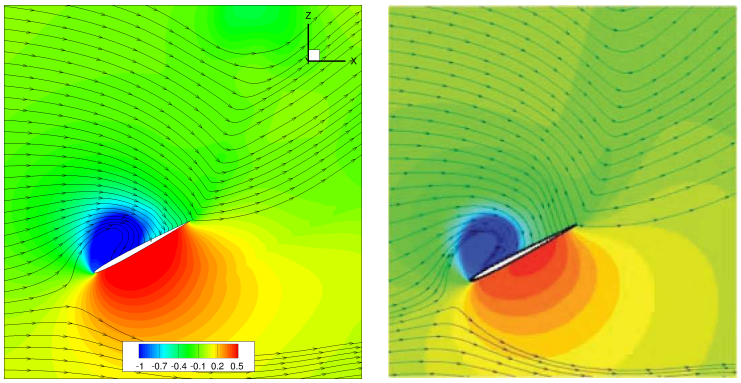

(g) t=3T/8, Present (h) t=3T/8, Yuan et al.

Figure 3. Pressure contours at reference section for 3D root flapping case (rigid wing).

and reference velocity). This simulation is done using a two mesh overset system consisting of a body-fitted curvilinear wing mesh overlayed onto a Cartesian background mesh.

Figures 2(a) and 2(b), respectively, show the variation of lift (C_L) and drag (C_D) coefficients with time. Note that the lift and drag coefficients were obtained by normalization with the wing planform area and reference velocity (described earlier). These results were compared with the experimental and CFD results of Yuan et al.[8] As can be seen in the figure, the current results correlate well with the numerical results of Yuan et al.[8] When both the computational results are compared with the experimental data, there is satisfactory agreement between the results. However, there are some differences in the computed magnitude of the secondary peak found in the lift time history when compared to that in the experimental data. The reason for these differences between the computational and the experimental results is not clear at this point.

Looking at the variation of drag with time, we can see that it has a negative value at all times, thus producing a net thrust over a flap cycle. The net drag coefficient predicted from the current simulation is -0.38 and it lies within 10% of the experimental value. Figure 3 shows the pressure coefficient (normalized by reference velocity) contours at the reference section plotted at different instances in time as the wing moves from the topmost position to the bottommost position. Contour plots obtained from the current simulation are compared with those obtained by Yuan et al.[8] as a part of validation. Both the simulations clearly show the leading edge vortex created due to the low pressure.

IV. Structural Model Validation

First, validation of the non linear shell model in MBDyn was carried out against some static benchmark cases which required the shell model to undergo significantly large deformations. Results of this study are presented in a previous work.[28] This model is then validated for rotating and flapping plates against analysis and experiments done by Beerinder et al.[34] First, spin up motion of a cantilevered plate was studied as shown in Figure 4(a). The rotational speed of the plate is given by,

$$\omega = \begin{cases} \omega_s(\frac{t}{t_s} - \frac{1}{2\pi}\sin\frac{2\pi t}{t_s}) & \text{if } 0 \le t \le t_s \\ \omega_s & \text{if } t > t_s \end{cases}$$

The properties of the wing are: $E = 70$ GPa, $\rho = 3000\ kg/m^3$, $l = 1.0$ m, $b = 0.5$ m, $t = 0.0025$ m, $\nu = 0.3$. The rotational speed was ramped up to $\omega_s = 10$ rad/sec over 5 seconds. Good correlation of wing tip deflection was obtained with the analysis of Beerinder et al. as shown in Figure 4(b).

The shell model in MBDyn is then validated for a rectangular aluminum plate undergoing pure flap motion (Figure 5(a)). The properties of the plate are as follows: $E = 70$ GPa, $\rho = 2750\ kg/m^3$, $l = 0.089$ m, $b = 0.038$ m, $t = 0.00058$ m, $\nu = 0.3$.

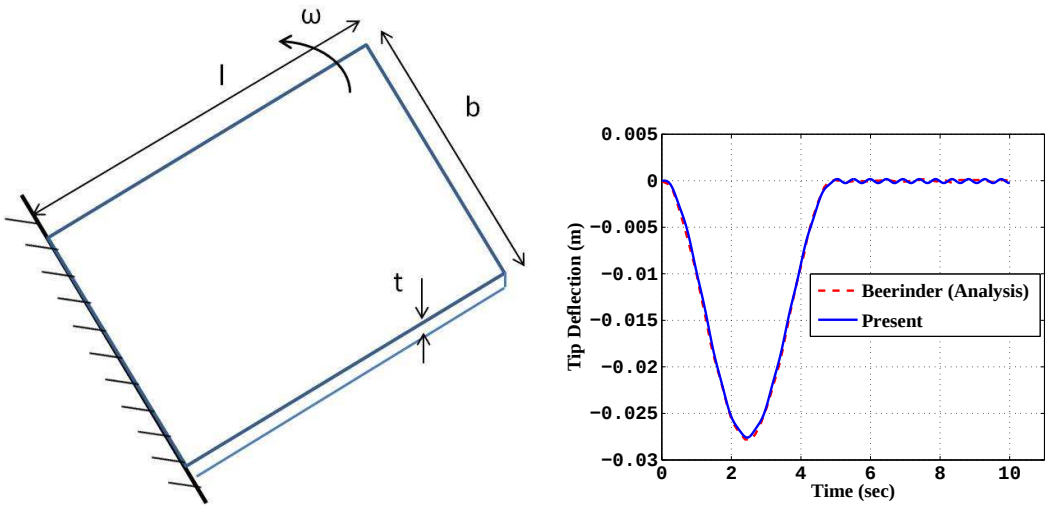

(a) Schematic (b) Tip deflection

Figure 4. Rotating cantilevered plate

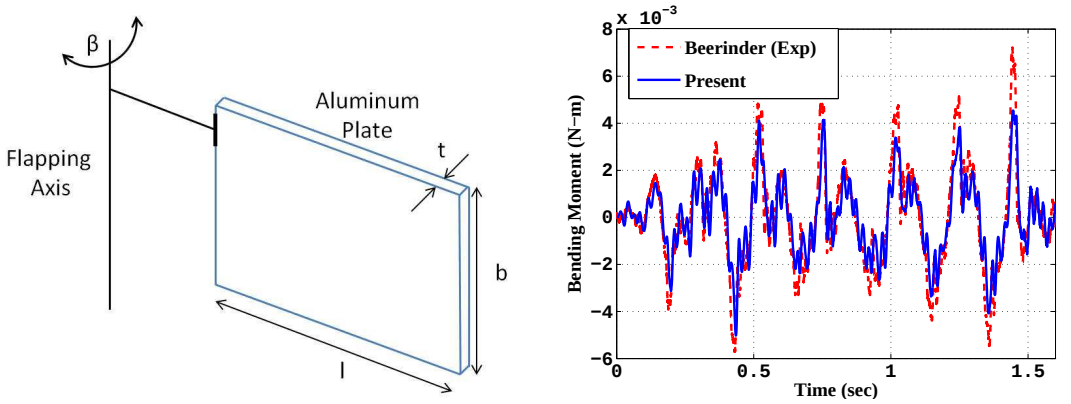

(a) Schematic

(b) Comparison of measured and predicted bending moment

Figure 5. Aluminum plate in pure flapping motion (slow support motion, flapping shaft shaken by hand)

Experimentally measured bending acceleration by Beerinder et al. was input into MBDyn and the bending moment at the base of the wing was compared with experiments. Comparison of prediction with experiments is shown in Figure 5(b) and satisfactory correlation is obtained.

V. CFD-CSD Validation

The focus of the current work is to validate the coupled CFD-CSD simulation for flexible flapping wings. In order to validate the coupled analysis, experiments carried out by Heathcote et al.[17] are simulated where the effect of spanwise flexibility on flapping wing aerodynamics was examined. Experiments were conducted in a water tunnel on a straight, untapered wing, in pure plunging motion at Reynolds numbers ranging from 10,000 to 30,000. Reduced frequencies up to about 5 were considered. For the present validation, focus is on cases at $Re = 30,000$ and $k = 1.82$ for which instantaneous force and tip displacements are available. Wings of 300 mm span, 100 mm chord, NACA0012 cross-section, and rectangular planform were used in the experiment. The model consisted of a rectangular stainless steel plate (Young's modulus, $E = 210$ GPa) of constant thickness, 1 mm. It was covered by a polydimethylsiloxane (PDMS) layer of very soft Young's modulus ($E = 250$ kPa), in order to reproduce the outer shape of the airfoil. The wing was designed to be stiff in the chordwise direction. In the experimental study, force measurements were made using strain gauges and wing deformations were captured using a motion tracking software. The root of the wing was subjected to a harmonic motion given by: $a_{root} = a_\circ \sin(\omega t)$, where $a_\circ = 0.175$ c, non dimensional root displacement amplitude. Experiments were also conducted on an inflexible wing, made as stiff as possible, using a nylon structure stiffened by thick steel rods.

A C-H grid is used to simulate the wing having 277 points in the wrap around, 81 points in the spanwise

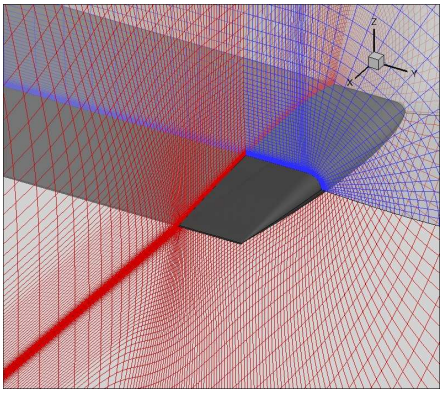

Figure 6. Grid for spanwise flexible wing

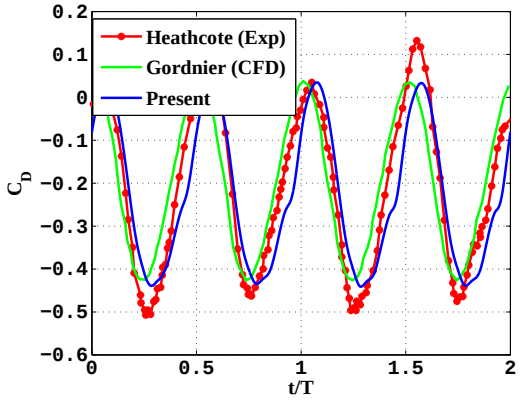

Figure 7. C_D **variation with time for rigid wing**

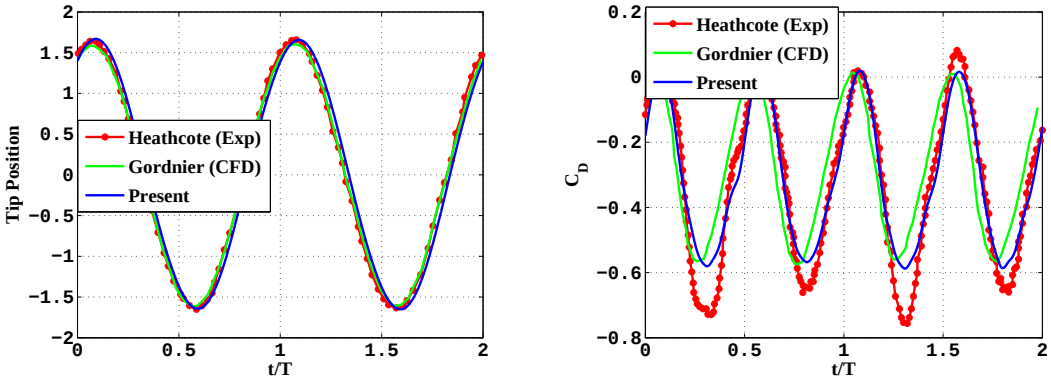

(a) Tip displacement at mid chord for flexible wing.

(b) C_D variation with time for flexible wing.

Figure 8. Instantaneous tip deflection and C_D **variation for for spanwise flexible wing**

and 85 points in the normal directions as shown in Figure 6. The main structural component of this model consists of a flat metal plate. Thus, it is modeled here using a single layer of nonlinear shell elements, and actuated by prescribing the heave motion of the semi-span wing root. The structural model consists of 5×15 shell elements respectively, in the chordwise and spanwise directions. These experiments have been used for validation in previous studies as well.[15,16] Results from the present study are compared with those of Gordnier et al.[15] They used a high-order Navier-Stokes solver coupled with a structural solver that decomposes the equations of three-dimensional elasticity into cross-sectional, small deformation and spanwise, large-deformation analyses for slender wings.

Figure 7 shows the instantaneous drag variation over two flap cycles for the rigid wing, starting from the top most position of the flap cycle for the rigid wing. In the present analysis, the inflexible wing is modeled using an ideally rigid model. From the figure, it can be seen that the instantaneous drag is negative throughout the flap cycle, thus implying a net thrust due to plunging motion. The present simulation resulted in an average C_T of 0.21, which is equal to the experimental value, as compared to 0.195 from the simulation by Gordnier et al.[15] These results further validate the CFD solver. Note that, Heathcote et al.[17] have not presented the instantaneous lift values and therefore, a comparison of the lift variation is not shown.

Figure 8(a) shows the instantaneous tip position at mid chord normalized by the root amplitude for the flexible wing. Due to spanwise flexibility, tip deflections are higher than the prescribed root motion. Figure 8(b) shows the instantaneous drag over the flap cycle for flexible wing. As compared to the rigid wing, higher propulsive thrust (negative drag) is obtained due to flexibility of the wing. The present simulation resulted in an average C_T of 0.31 as compared to the experimental C_T of 0.32, and 0.278 from the simulation by Gordnier et al.[15] Therefore, due to flexibility, the average C_T increased by 47%.

Figures 9 and 10 show the comparison of vortical wake structures between the results by Gordnier et

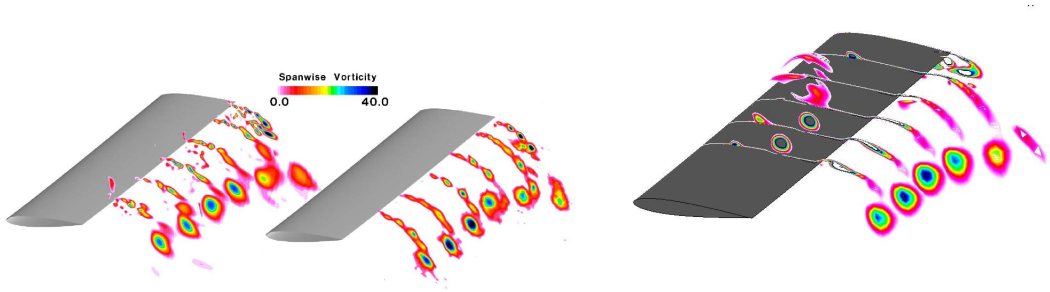

(a) Gordnier et al.[15] (left), Heathcote et al.[17] (right) (b) Present

Figure 9. Comparison of wake structure at various spanwise stations at the peak of the upstroke, $t/T = 0.0$ for spanwise flexible wing

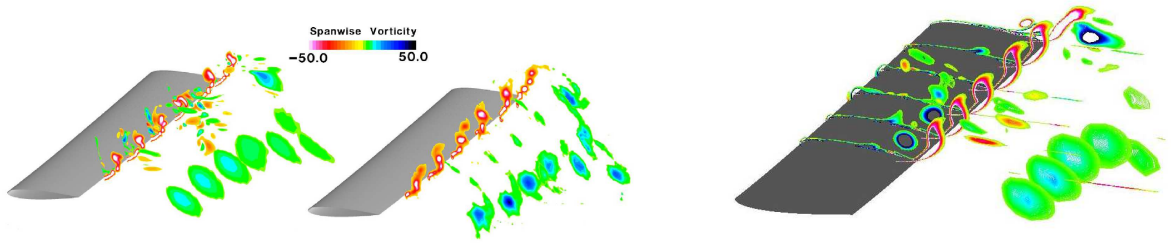

(a) Gordnier et al.[15] (left), Heathcote et al.[17] (right) (b) Present

Figure 10. Comparison of wake structure at various spanwise stations at the midpoint of the downstroke, $t/T = 0.25$ for spanwise flexible wing

al.,[15] experiments by Heathcote et al.[17] and present simulation. Similar vortical structures are obtained as compared to prior research at two instants of time, $t/T = 0$ and $t/T = 0.25$, respectively.

Figure 11 shows the spanwise vorticity contours and surface pressure contours for the rigid and flexible wings (starting from the top most position in plunge cycle). Since this case is a pure plunge motion, for the rigid case, the flow is mostly 2D till about 75% span location. Beyond this the flow becomes 3D due to the tip effect. On the other hand, for the flexible case, since there is flap bending and the plunge amplitude varies over the span, the 2D nature is not preserved even at further inboard locations. The flow is more 3-D in the flexible wing case as compared to the rigid wing. As compared to the rigid wing, since the flexible wing has higher plunge amplitude near the wing tip, this leads to a higher effective angle of attack and higher propulsive thrust and lift. The leading edge vortices are stronger towards the outboard sections of the wing and also the strength of the tip vortex is higher. These observations are consistent with those made by Gordnier et al.[15]

Figure 12 shows the instantaneous lift variation over the flap cycle for the rigid and flexible wings. Due to symmetry in the upstroke and downstroke, the average lift in this case is zero. However, due to flexibility, the maximum instantaneous lift value is increased from 4.4 in case of a rigid wing, to 5.6 for the flexible wing. Figure 13 shows the spanwise C_l and C_d variation for the rigid and flexible wings at the same instant of time (t/T=0.25, middle of downstroke). Sectional lift is higher for flexible wing, particularly towards the outer sections of the wing. Similar trend is seen for negative drag or thrust.

VI. Investigation of a Chordwise Flexible Wing

A chordwise flexible wing is simulated to further demonstrate the capability of the CFD-CSD solver. Note that there is no reliable experimental data available for validation. Therefore, the current analysis is done based on a simulation by Gopalakrishnan et al.[18] The simulation by Gopalakrishnan et al. is performed on rigid as well as flexible root flapping wings by coupling an LES solver to a linear elastic membrane model. It should be noted that they studied the effect of prestress on flexible wing performance, but used a linear assumption for the prestress values. The present study is not limited to analyzing membrane models linearized about a prestressed condition, but allows the prestress to change accordingly. This is expected

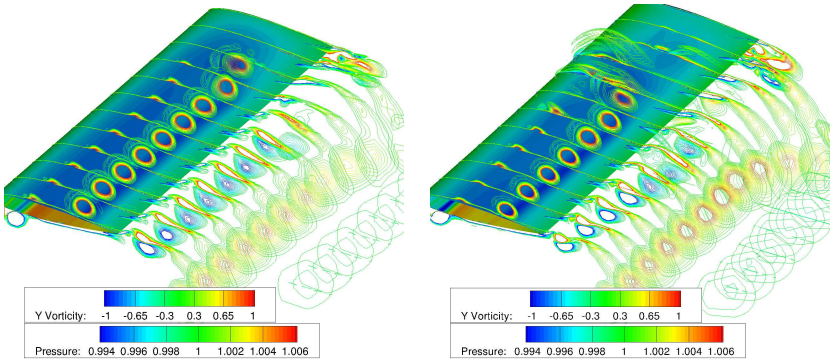

(a) t=0, Rigid (b) t=0, Flexible

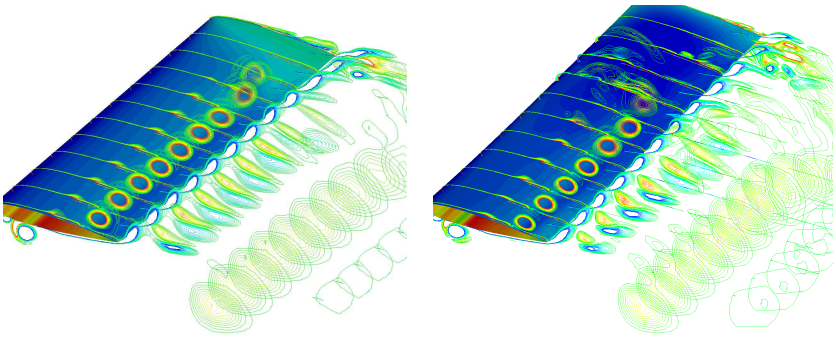

(c) t=T/8, Rigid (d) t=T/8, Flexible

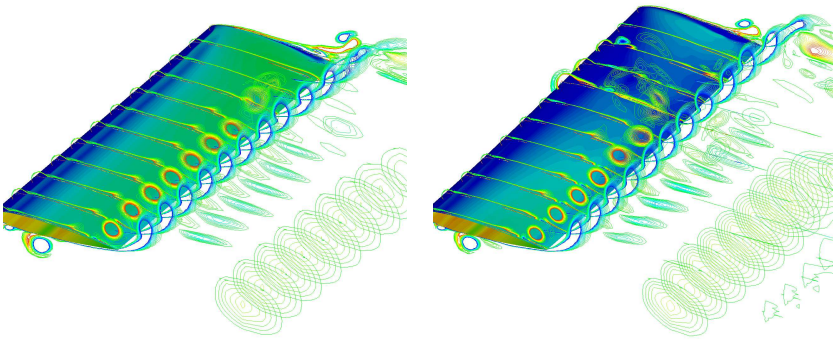

(e) t=T/4, Rigid (f) t=T/4, Flexible

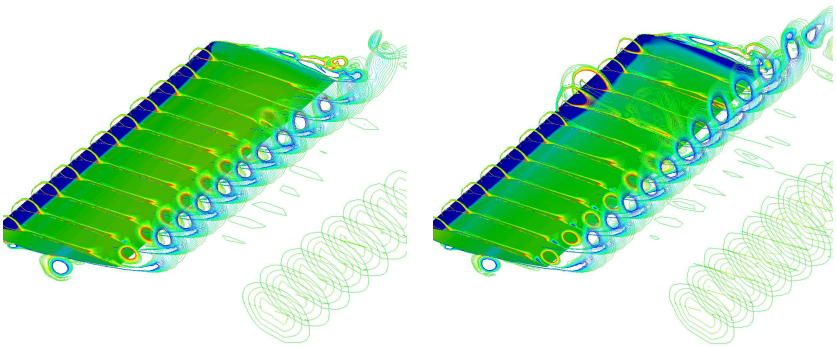

(g) t=3T/8, Rigid (h) t=3T/8, Flexible

Figure 11. Y vorticity contours for rigid and spanwise flexible wings.

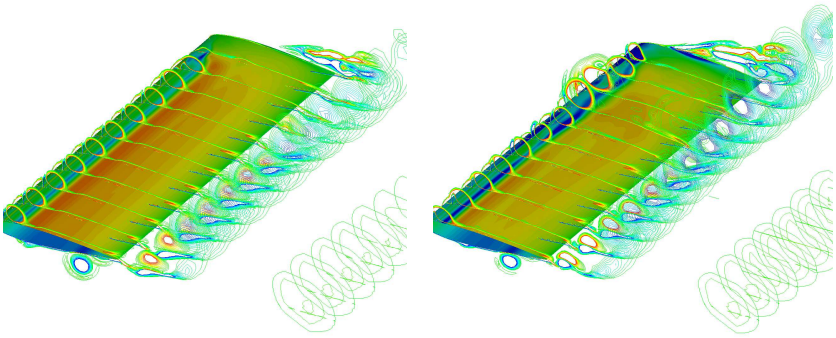

(i) t=T/2, Rigid (j) t=T/2, Flexible

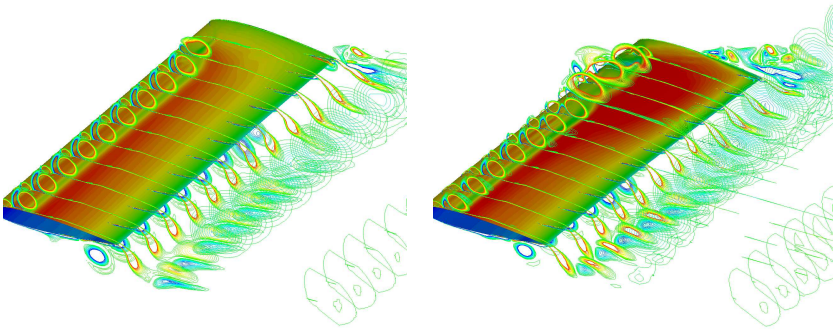

(k) t=5T/8, Rigid (l) t=5T/8, Flexible

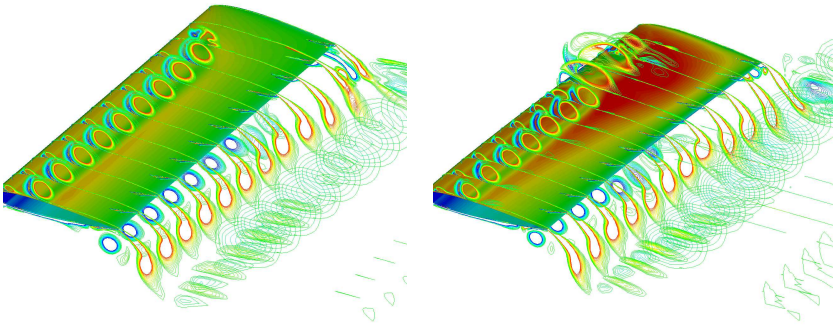

(m) t=3T/2, Rigid (n) t=3T/2, Flexible

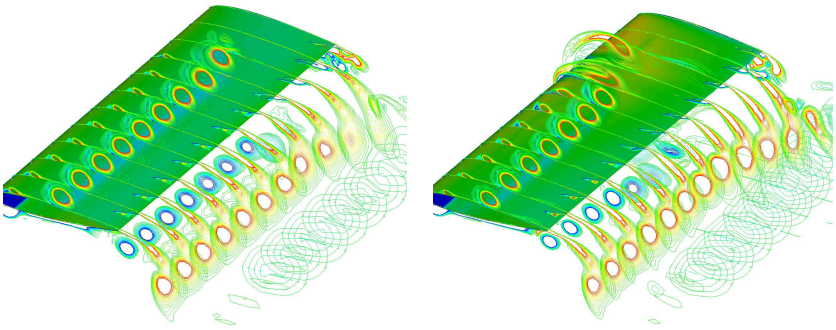

(o) t=7T/8, Rigid (p) t=7T/8, Flexible

Figure 11. Y vorticity contours for rigid and spanwise flexible wings (continued).

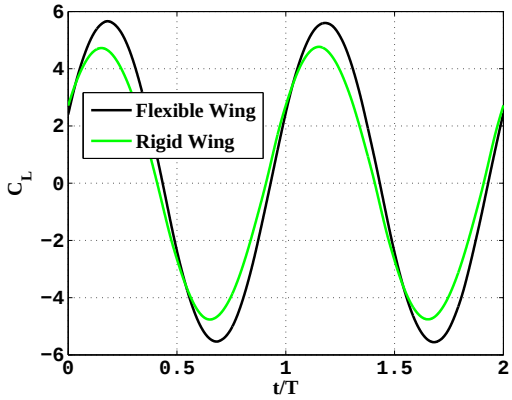

Figure 12. C_L **variation with time for rigid and spanwise flexible wings.**

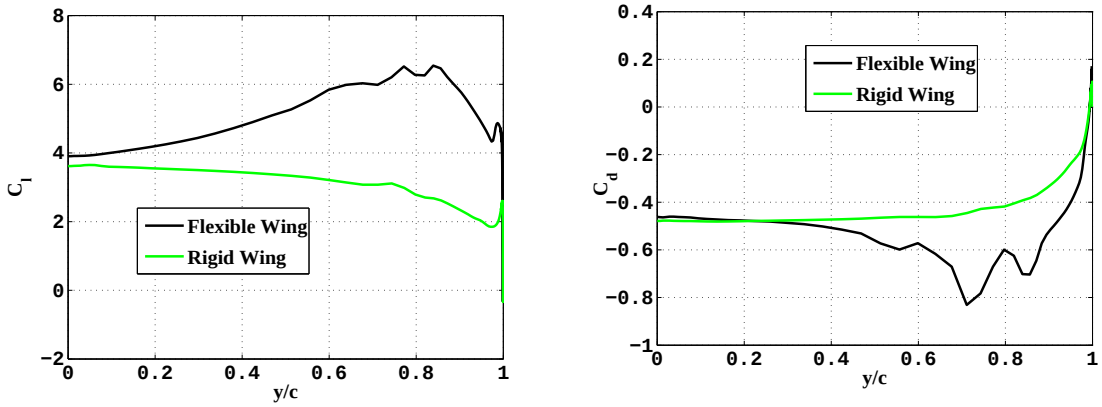

(a) C_l (b) C_d

Figure 13. Spanwise C_l **and** C_d **variation for rigid and spanwise flexible wings at** $t/T = 0.25$

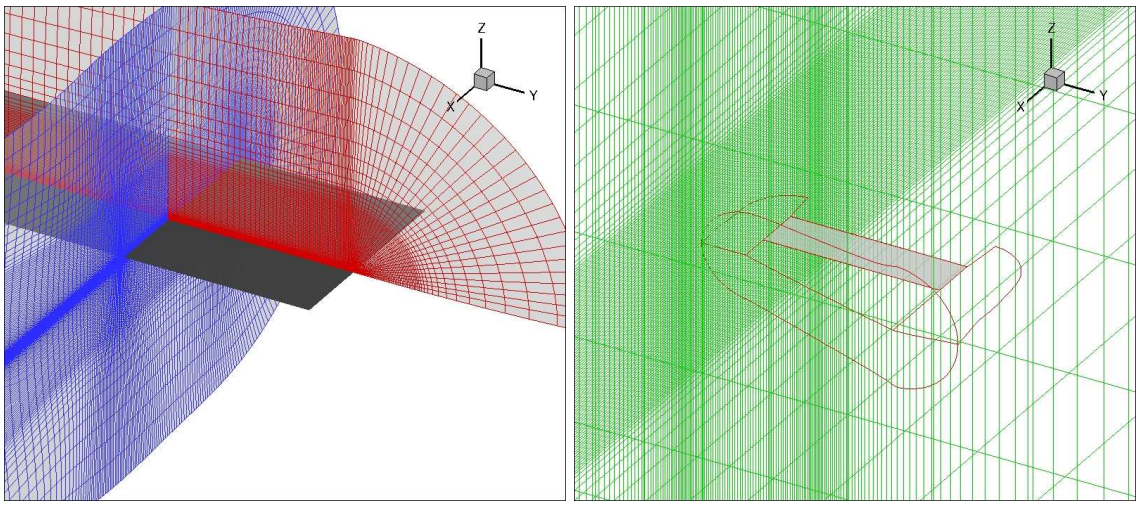

(a) Blade mesh ($267 \times 181 \times 85$) (b) Cartesian background mesh ($162 \times 195 \times 122$) with wing mesh boundary

Figure 14. Computational mesh for 3D root flapping chordwise flexible wing simulation.

to improve the quality of the analysis compared to current literature. Therefore, we are not comparing the

flexible wing results from the present study with those of Gopalakrishnan et al.,[18] but instead just compare results of the flexible wing with those of rigid wing.

The wing considered is a rectangular wing with an aspect ratio of 4 and root cutout of 0.5 chord. The wing thickness to chord ratio was 0.00125. Flapping frequency is 11.94 Hz and Reynolds number of the flow is $10,000$. The pitching axis is placed at one-fourth of a chord length from the leading edge. The wing is held fixed at the root and flapped with the following parameters:

Flap: $\gamma = \gamma_o \cos(2 \cdot \pi f \cdot t)$,

Pitch: $\theta = \theta_o - \theta_a \sin(2 \cdot \pi f \cdot t)$

with $\gamma_o = 30^o$, $\theta_o = 12.5^o$, $\theta_a = 32.5^o$

A two mesh overset system consisting of a body-fitted curvilinear wing mesh overlayed onto a Cartesian background mesh is used for this case. The wing mesh has clustering at the wing root and tip as well as leading and trailing edges. The Cartesian background mesh is refined to resolve tip vortex evolution. The wing mesh has 267 points in the wrap around, 181 points in the spanwise and 85 points in the normal directions. The Cartesian background mesh has 162 points in the streamwise, 195 points in the spanwise and 122 points in the vertical directions. The mesh for this case is shown in Figure 14.

Figure 15 shows the rigid wing results from the present study and the simulation by Gopalakrishnan et al.[18] and satisfactory correlation is achieved. The average C_L and C_T values are 1.9 and 1.2, respectively. A membrane model is then used to analyze a chordwise flexible wing with no prestress. The Young's Modulus is $E = 2 * 10^6\ N/m^2$ and density of the material, $\rho_w = 1350\ kg/m^3$. As a result of this flexibility, the wing produced a positive camber during the downstroke and negative camber during the upstroke over a large portion of the wing. A side view of the wing during the middle of the downstroke is shown in Figure 16.

Figures 17(a) and 17(b) show the instantaneous drag and lift, respectively, for the rigid and flexible wings. The average C_L increased by 10% to 2.1 and the average C_T increased by 25% to 1.5 due to flexibility in the wing. Figure 18 shows the spanwise variation of C_l and C_d for the rigid and flexible wings at the same instant

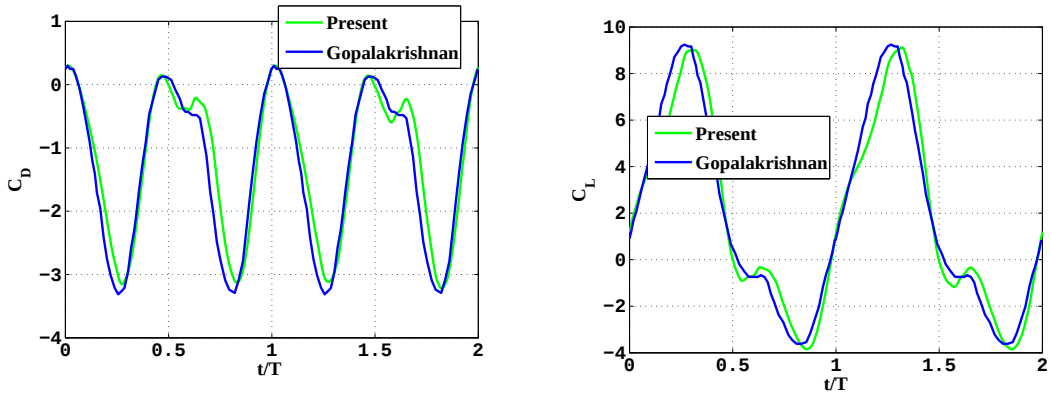

(a) C_D (b) C_L

Figure 15. C_D and C_L variation with time for 3D root flapping chordwise rigid case

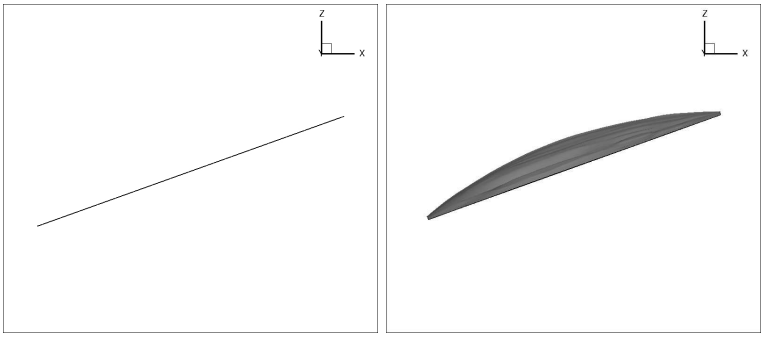

(a) Rigid Wing (b) Flexible Wing

Figure 16. Side view of rigid and chordwise flexible wings at $t/T = 0.25$.

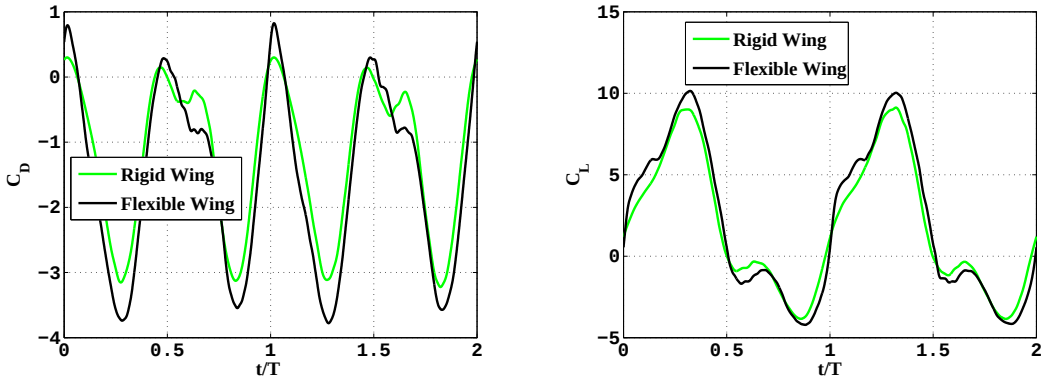

(a) C_D (b) C_L

Figure 17. C_D **and** C_L **variation with time for 3D root flapping chordwise flexible case**

of time (t/T=0.25, middle of downstroke). Similar to the spanwise flexible wing, the chordwise flexible wing has higher sectional C_l and negative C_d towards the tip. Figure 19 shows the comparison between the surface pressure contours for the rigid and flexible wings at 3/4th spanwise location for various instants of time. Due to the camber that develops for the flexible wing, a greater portion of the resultant force is vectored in the chordwise direction. Also, the strength of leading edge suction is higher in the flexible wing case. This clearly shows the beneficial effect of flexibility on the aerodynamics of flapping wings.

VII. Conclusion

A coupled CFD-CSD solver was used to simulate the aerodynamics of a flexible flapping wing. The CFD solver was a compressible RANS solver, which was first validated for rigid 2D and 3D wings. Good correlation was obtained for all the cases considered. The structural solver used is called MBDyn which has been extended to take into account non linear shell straining, making it possible to analyze plates with large deformations. It was validated with prior research on rotating and flapping plates.

Finally, validation of the aeroelastic solver was carried out. A spanwise flexible wing was simulated and good correlation was obtained with prior experiments and CFD analysis. It was observed that due to flexibility, the chordwise propulsive force increases as a result of increase in plunge amplitude, effective angle of attack and leading edge suction. Then, a chordwise flexible wing was analyzed using the solver. This was a root flap case where the wing was held fixed at the root and flapped. As a result of the flexibility, camber was produced towards outer sections of the wing as it flapped. Highly 3D flow was observed with strength

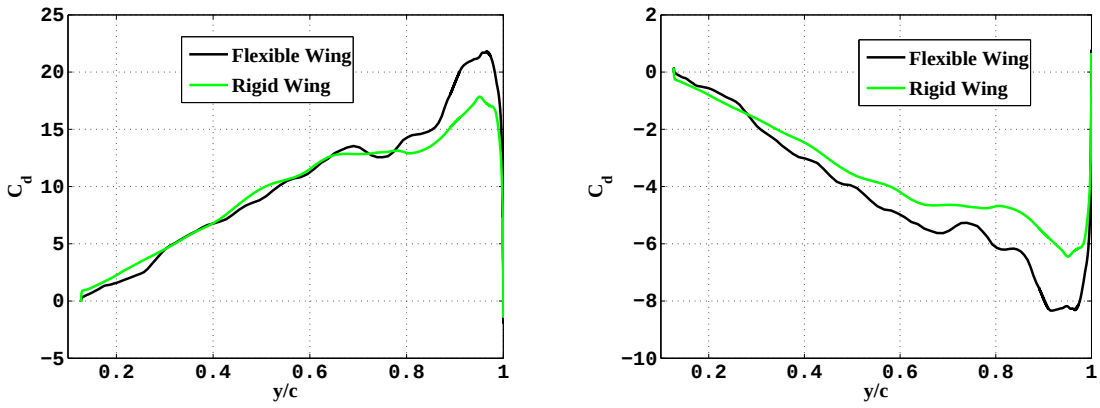

(a) C_l (b) C_d

Figure 18. Spanwise C_l **and** C_d **variation for rigid and chordwise flexible wings at** $t/T = 0.25$

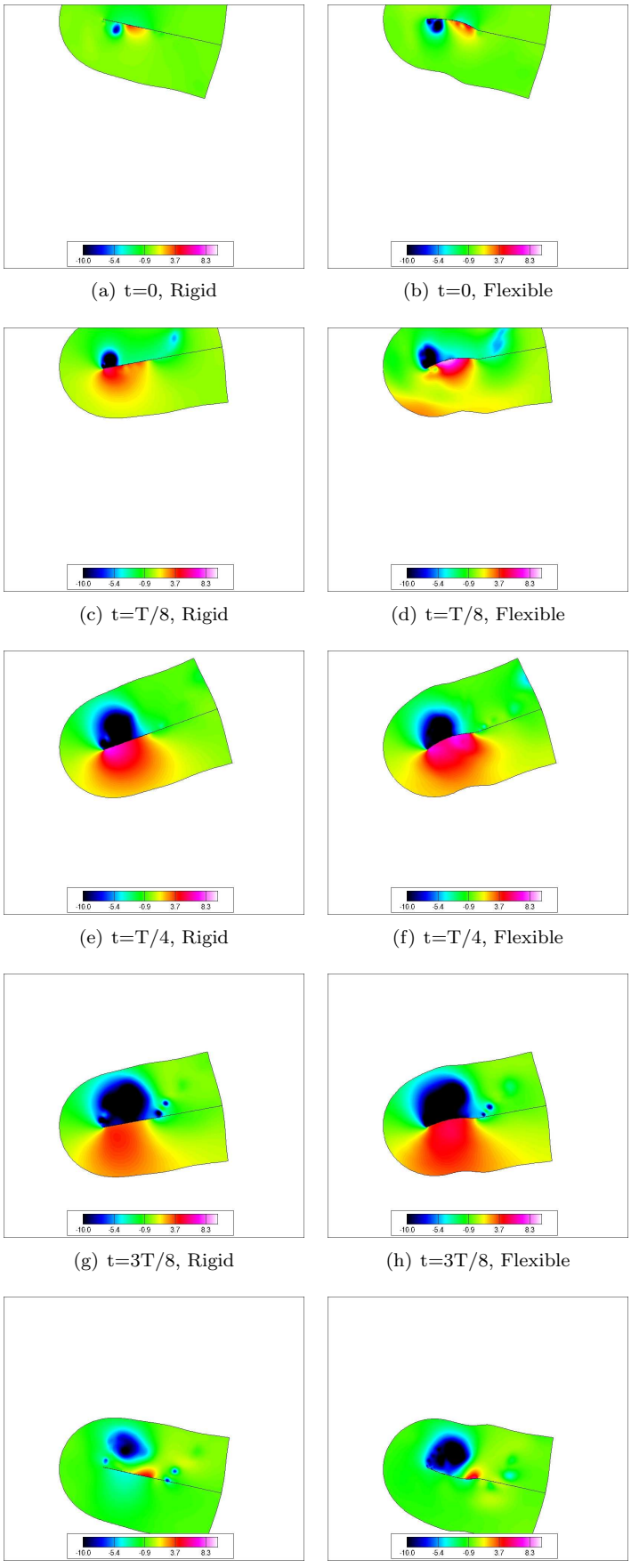

(a) t=0, Rigid (b) t=0, Flexible

(c) t=T/8, Rigid (d) t=T/8, Flexible

(e) t=T/4, Rigid (f) t=T/4, Flexible

(g) t=3T/8, Rigid (h) t=3T/8, Flexible

(i) t=T/2, Rigid (j) t=T/2, Flexible

Figure 19. Pressure contours at 3/4th spanwise section for rigid and chordwise flexible wings.

of the vortices increasing from root to tip. Due to camber in the wing, the resultant force was vectored more in the chordwise direction as compared to rigid wings, which resulted in higher thrust.

As a concluding remark, the current work demonstrates the capability of an aeroelastic solver to characterize the flowfield of a flexible flapping wing MAV in 3D. Future work will include examining the various parameters like the wing stiffness parameters, wing geometry and flapping kinematics which can be optimized to design a flapping wing MAV.

Acknowledgments

This research was supported by the Armys MAST CTA Center for Microsystem Mechanics with Mr. Chris Kroninger (ARL-VTD) as Technical Monitor.

References

[1]Chopra, I., "Hovering Micro Air Vehicles: Challenges and Opportunities," Proceedings of AHS International Meeting on Advanced Rotorcraft Technology and Safety Operations (Heli Japan), Sonic City, Ohmiya, Japan, November 2010.

[2]Knoller, R., "Die Gesetze des Luftwiderstandes," Flug- und Motortechnik (Wien), Vol. 3, (21), 1909, pp. 1–7.

[3]Betz, A., "Ein Beitrag zur Erklaerung des Segelfluges," Zeitschrift fur Flugtechnik und Motorluftschiffahrt, Vol. 3, 1912, pp. 269–272.

[4]Katzmayr, R., "Effect of Periodic Changes of Angle of Attack on Behavior of Airfoils," NACA TM 147, Oct. 1922.

[5]McCroskey, W.J., "Unsteady Airfoils," *Annual Review Fluid Mechanics*, Vol. 14, 1982, pp. 285–311.

[6]Carr, L., "Progress in Analysis and Prediction of Dynamic Stall," *Journal of Aircraft*, Vol. 25, 1988, pp. 6–17.

[7]Hart, A. and Ukeiley, L., "Low Reynolds Number Unsteady Aerodynamics over a Pitching-Plunging Flat Plate," AIAA Paper 2010–387, January 2010.

[8]Yuan, W., Lee, R., Hoogkamp, E., Khalid, M., "Numerical and Experimental Simulations of Flapping Wings," *International Journal of Micro Air Vehicles*, Vol. 2, (3), September 2010, pp. 181–209.

[9]Wang, H., Zeng, L., Liu, H., Yin, C., "Measuring Wing Kinematics, Flight Trajectory and Body Attitude During Forward Flight and Turning Maneuvers in Dragonflies," *The Journal of Experimental Biology*, Vol. 206, 2003, pp. 745–757.

[10]Malhan, R., Benedict, M., Chopra, I., "Experimental Investigation of a Flapping Wing Concept in Hover and Forward Flight for Micro Air Vehicle Applications," Proceedings of the 66th Annual American Helicopter Society Forum, Phoenix, Az, May 2010.

[11]Wu, P., Ifju P., Stanford B., "Flapping Wing Structural Deformation and Thrust Correlation Study with Flexible Membrane Wings," *AIAA Journal*, Vol. 48, (9), Sept. 2010, pp. 2111–2122.

[12]Tuncer, I. H., Platzer, M. F., "Thrust Generation Due to Airfoil Flapping," *AIAA Journal*, Vol. 34, (2), Feb. 1996, pp. 324–331.

[13]Tuncer, I. H., Walz, R., Platzer, M. F., "A Computational Study of the Dynamic Stall of a Flapping Airfoil," AIAA Paper 98–2519, June 1998.

[14]Isogai, K., Shinmoto, Y., Watanabe, Y., "Effects of Dynamic Stall on Propulsive Efficiency and Thrust of Flapping Airfoil," *AIAA Journal*, Vol. 37, (10), Oct. 1999, pp. 1145–1151.

[15]Chimakurthi, S. K., Tang, J., Palacios, R., Cesnik, C. E. S., Shyy, W., "Computational Aeroelasticity Framework for Analyzing Flapping Wing Micro Air Vehicles," *AIAA Journal*, Vol. 47, No. 8, August 2009, doi:10.2514/1.38845.

[16]P. Masarati, M. Morandini, G. Quaranta, D. Chandar, B. Roget, J. Sitaraman, "Tightly Coupled CFD/Multibody Analysis of Flapping-Wing MAV," 41st AIAA Fluid Dynamics Conference, 2011, Honolulu, Hawaii, USA.

[17]Heathcote, S., Wang, Z., Gursul, I., "Effect of Spanwise Flexibility on Flapping Wing Propulsion," Journal of Fluids and Structures, Vol. 24, No. 2, February 2008, pp. 183–199, doi:10.1016/j.jfluidstructs.2007.08.003.

[18]Gopalakrishnan, P., Tafti, D. K., "Effect of Wing Flexibility on Lift and Thrust Production in Flapping Flight," *Journal of Aircraft*, Vol. 48, No. 5, May 2010.

[19]Lakshminarayan, V. K., Baeder, J. D., "Computational Investigation of Micro Hovering Rotor Aerodynamics," *Journal of the American Helicopter Society*, Vol. 55, (2), April 2010.

[20]Lakshminarayan, V. K., Baeder, J. D., "Computational Investigation of Micro-Scale Coaxial Rotor Aerodynamics in Hover," *Journal of Aircraft*, Vol. 47, (3), June 2010, pp. 940–955.

[21]Lakshminarayan, V. K., "Computational Investigation of Micro-Scale Coaxial Rotor Aerodynamics in Hover," *Ph.D. Dissertation*, Department of Aerospace Engineering, University of Maryland at College Park, 2009.

[22]Malhan, R., Lakshminarayan, V., Baeder, J., Chopra, I., "Investigation of Aerodynamics of Rigid Flapping Wings for MAV Applications: CFD Validation," American Helicopter Society Specialists Conference on Unmanned Rotorcraft and Network Centric Operations, Tempe, Az, Jan 2011.

[23]Pulliam, T., Chaussee, D., "A Diagonal Form of an Implicit Approximate Factorization Algorithm," *Journal of Computational Physics*, Vol. 39, (2), February 1981, pp. 347–363.

[24]Buelow P. E. O., Schwer D. A., Feng J., Merkle C. L., "A Preconditioned Dual-Time, Diagonalized ADI scheme for Unsteady Computations," AIAA paper 1997–2101, 13th AIAA Computational Fluid Dynamics Conference, Snowmass Village, CO, July 1997.

[25]Pandya, S. A., Venkateswaran, S., Pulliam, T. H., "Implementation of Preconditioned Dual-Time Procedures in OVERFLOW," AIAA paper 2003–0072, 41st AIAA Aerospace Sciences Meeting and Exhibit, Reno, NV, January 2003.

[26]Spalart, P.R., Allmaras, S.R., "A One-equation Turbulence Model for Aerodynamic Flows," AIAA Paper 1992–0439, 30th AIAA Aerospace Sciences Meeting and Exhibit, Reno, NV, January 1992.

[27]Lee, Y., "On Overset Grid Connectivity and Automated Vortex Tracking in Rotorcraft," *Ph.D Dissertation*, Department of Aerospace Engineering, University of Maryland at College Park, 2008.

[28]Masarati, P., Morandini, M., Quaranta, G., Vescovini, R., "Multibody Analysis of a Micro-Aerial Vehicle Flapping Wing," Multibody Dynamics 2011, edited by J. C. Samin and P. Fisette, Brussels, Belgium, July 2011.

[29]Masarati, P. Sitaraman, J., "Tightly Coupled CFD/Multibody Analysis of NREL Unsteady Aerodynamic Experiment Phase VI Rotor," 49th AIAA Aerospace Sciences Meeting, Orlando, Florida, January 2011.

[30]Baron, A., Boffadossi, M., De Ponte, S., "Numerical Simulation of Vortex Flows Past Impulsively Started Wings," AGARD-CP-494 Vortex Flow Aerodynamics, 1990, pp. 33/1–33/14.

[31]Ghiringhelli, G., L., Masarati, P., Mantegazza, P., "A Multi-Body Implementation of Finite Volume Beams," *AIAA Journal*, Vol. 38, (1), January 2000, pp. 131–138.

[32]Farhat, C., Lesoinne, M., "Two efficient staggered algorithms for the serial and parallel solution of three-dimensional nonlinear transient aeroelastic problems," Computer Methods in Applied Mechanics and Engineering, 182:499–515, 2000.

[33]Quaranta, G., Masarati, P., Mantegazza, P., "A Conservative Mesh-Free Approach for Fluid Structure Interface Problems," Coupled Problems 2005, Santorini, Greece, May 2005.

[34]Singh, B., "Dynamics and Aeroelasticity of Hover Capable Flapping Wings: Experiments and Analysis," *Ph.D Dissertation*, Department of Aerospace Engineering, University of Maryland at College Park, 2006.